Article:
Pearson, Caroline, Tindall, Sarah, Herman, Reyme et al. (2020) Acetylation of surface carbohydrates in bacterial pathogens requires coordinated action of a two-domain membrane-bound acyltransferase. MBio. e01364-20. pp. 1-19. ISSN: 2150-7511

https://doi.org/10.1128/mBio.01364-20

AMERICAN SOCIETY FOR MICROBIOLOGY | mBio®

RESEARCH ARTICLE
Molecular Biology and Physiology

Acetylation of Surface Carbohydrates in Bacterial Pathogens Requires Coordinated Action of a Two-Domain Membrane-Bound Acyltransferase

Caroline R. Pearson,[a,b] Sarah N. Tindall,[a,b] Reyme Herman,[b] Huw T. Jenkins,[d] Alex Bateman,[e] Gavin H. Thomas,[a,b] Jennifer R. Potts,[b] Marjan W. Van der Woude[a,c]

[a]York Biomedical Research Institute, University of York, York, United Kingdom
[b]Department of Biology, University of York, York, United Kingdom
[c]Hull York Medical School, University of York, York, United Kingdom
[d]York Structural Biology Laboratory, Department of Chemistry, University of York, York, United Kingdom
[e]European Molecular Biology Laboratory, European Bioinformatics Institute (EMBL-EBI), Wellcome Genome Campus, Hinxton, Cambridgeshire, United Kingdom

Caroline R. Pearson and Sarah N. Tindall contributed equally to this work. Author order was determined alphabetically.

ABSTRACT Membrane bound acyltransferase-3 (AT3) domain-containing proteins are implicated in a wide range of carbohydrate O-acyl modifications, but their mechanism of action is largely unknown. O-antigen acetylation by AT3 domain-containing acetyltransferases of *Salmonella* spp. can generate a specific immune response upon infection and can influence bacteriophage interactions. This study integrates *in situ* and *in vitro* functional analyses of two of these proteins, OafA and OafB (formerly F2GtrC), which display an "AT3-SGNH fused" domain architecture, where an integral membrane AT3 domain is fused to an extracytoplasmic SGNH domain. An *in silico*-inspired mutagenesis approach of the AT3 domain identified seven residues which are fundamental for the mechanism of action of OafA, with a particularly conserved motif in TMH1 indicating a potential acyl donor interaction site. Genetic and *in vitro* evidence demonstrate that the SGNH domain is both necessary and sufficient for lipopolysaccharide acetylation. The structure of the periplasmic SGNH domain of OafB identified features not previously reported for SGNH proteins. In particular, the periplasmic portion of the interdomain linking region is structured. Significantly, this region constrains acceptor substrate specificity, apparently by limiting access to the active site. Coevolution analysis of the two domains suggests possible interdomain interactions. Combining these data, we propose a refined model of the AT3-SGNH proteins, with structurally constrained orientations of the two domains. These findings enhance our understanding of how cells can transfer acyl groups from the cytoplasm to specific extracellular carbohydrates.

IMPORTANCE Acyltransferase-3 (AT3) domain-containing membrane proteins are involved in *O*-acetylation of a diverse range of carbohydrates across all domains of life. In bacteria they are essential in processes including symbiosis, resistance to antimicrobials, and biosynthesis of antibiotics. Their mechanism of action, however, is poorly characterized. We analyzed two acetyltransferases as models for this important family of membrane proteins, which modify carbohydrates on the surface of the pathogen *Salmonella enterica*, affecting immunogenicity, virulence, and bacteriophage resistance. We show that when these AT3 domains are fused to a periplasmic partner domain, both domains are required for substrate acetylation. The data show conserved elements in the AT3 domain and unique structural features of the periplasmic domain. Our data provide a working model to probe the mechanism and function of the diverse and important members of the widespread AT3 protein

Citation Pearson CR, Tindall SN, Herman R, Jenkins HT, Bateman A, Thomas GH, Potts JR, Van der Woude MW. 2020. Acetylation of surface carbohydrates in bacterial pathogens requires coordinated action of a two-domain membrane-bound acyltransferase. mBio 11:e01364-20. https://doi.org/10.1128/mBio.01364-20.

Invited Editor Anthony J. Clarke, University of Guelph

Editor Gerald B. Pier, Harvard Medical School

Address correspondence to Marjan W. Van der Woude, Marjan.vanderwoude@york.ac.uk.

Received 27 May 2020
Accepted 10 July 2020
Published 25 August 2020

family, which are required for biologically significant modifications of cell-surface carbohydrates.

KEYWORDS O-antigen, SGNH superfamily, *Salmonella*, acetylation, acyltransferase-3 family, Gram-negative bacteria, lipopolysaccharide, membrane proteins, structure-activity relationship, surface antigens

Salmonella infections are a considerable public health burden in both developing and developed countries. *Salmonella enterica* subspecies *enterica* serovar Typhimurium is estimated to cause more than 150,000 human deaths from gastroenteritis each year (1, 2). A sublineage of this serovar is the dominant cause of invasive nontyphoidal *Salmonella* (iNTS) bloodstream infections in Africa (3). The Typhi serovar of this subspecies is the major cause of typhoid fever, resulting in over 200,000 deaths annually (2, 4). In the United States, there are over 10,000 cases annually of these serovars combined (5, 6).

Cell surface lipopolysaccharide (LPS) is an important virulence factor. The O-antigen, the most distal and variable portion of LPS, is composed of repeating oligosaccharide units whose composition and structure vary between species and, in the case of *Salmonella* spp., between serovars. Modification of the O-antigen by alteration of sugar linkages or addition of moieties such as glucose or acetate (7, 8) can influence immunogenicity and virulence, and confer resistance to lytic phage infection (9–12).

Carbohydrates on the bacterial cell surface are frequently *O*-acetylated by acyltransferase proteins which contain a 10-transmembrane helix (TMH) acyltransferase-3 (AT3) (InterPro IPR002656 and Pfam PF01757; also known as acyltransferase_3/putative acetyl-CoA transporter, Transporter Classification Database number [TC] number 9.B.97). This family of proteins is widespread in eukaryotes and prokaryotes and is involved in a range of acylation modifications. Examples of AT3-containing acetyltransferases from prokaryotes include those mediating peptidoglycan acetylation and contributing to lysozyme resistance (13, 14), modification of root nodulation factors to initiate symbioses (15), and O-antigen acetylation (9, 16, 17). Despite the involvement of AT3-containing proteins in a wide range of reactions, their mechanism and structure are poorly characterized.

Among bacterial AT3 carbohydrate acetyltransferases, there are two known domain architectures, proteins consisting of an AT3 domain only (AT3-only) and an N-terminal AT3 domain linked to an extracytoplasmic domain, commonly an SGNH domain (AT3-SGNH fused). The SGNH domain is fused through addition of an 11th TMH and linking region. Oac (in *Shigella* spp.) is an example of an AT3-only protein that is essential for O-antigen acetylation (18), whereas OatA, the *O*-acetyltransferase of peptidoglycan in *Staphylococcus* spp., is an example of an AT3-SGNH fused protein (14). SGNH domains (InterPro number IPR036514) are a large and diverse family of small catalytic domains of around 200 amino acids, originally characterized as a subgroup of the GDSL hydrolase family based on their invariant residues, Ser, Gly, Asn, His—hence, SGNH—which occur in four blocks of conserved sequence (19, 20). Members of this family that are active against carbohydrates are also classified as CE3 family proteins in the carbohydrate-active enzymes database (CAZy) (21). Subsequently, many more proteins have been found to belong to this diverse family, and they no longer fully adhere to the original paradigm of SGNH. However, most members typically contain a catalytic triad of Ser, His, and Asp and oxyanion hole residues within the four blocks of conserved sequence (22). It is not clear how the AT3 and SGNH domains function together in AT3-SGNH fused carbohydrate acetyltransferases, nor how the AT3-only proteins function independently of a linked periplasmic domain.

In *Salmonella* spp., there are two defined O-antigen acetyltransferases, OafA and OafB (9, 10, 17, 23). Slauch et al. determined that the integral membrane protein OafA from *S.* Typhimurium (17) acetylates the 2-hydroxyl group on the abequose moiety of the O-antigen unique to this serovar (24). This results in acquisition of the O:5 serotype (defined by the Kauffmann-White-Le Minor scheme) (25, 26), which is required for

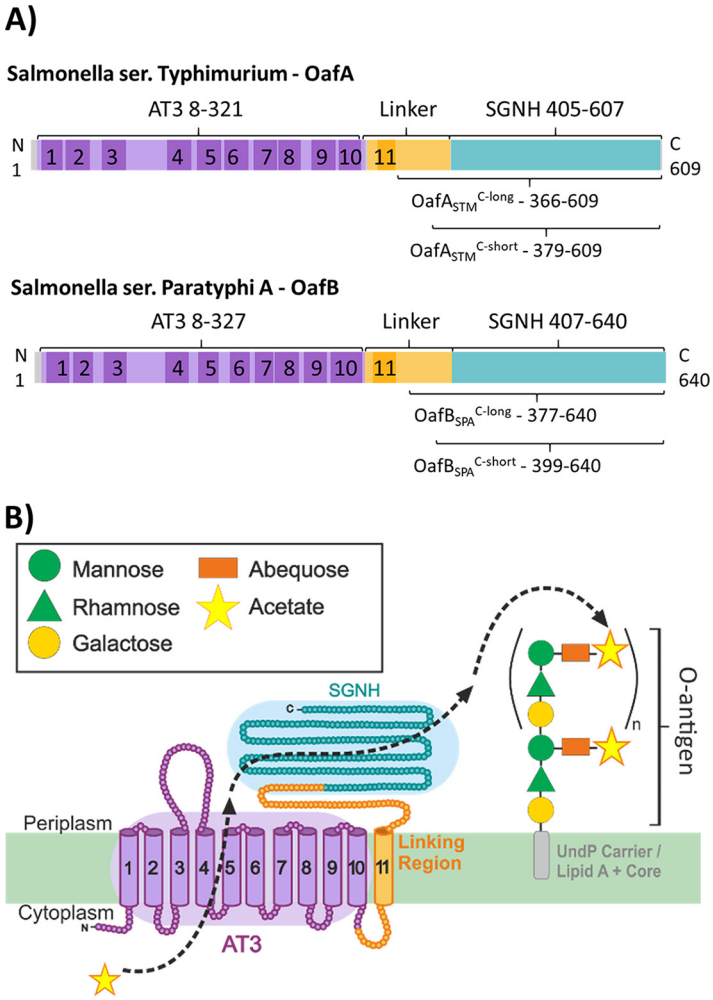

FIG 1 OafA and OafB are membrane-bound *O*-acetyltransferases that acetylate the O-antigen of *Salmonella*. (A) Schematic representation of OafA and OafB functional (colored) and transmembrane (shaded) domains predicted by InterPro and TMHMM, respectively. C-term constructs used for *in vitro* characterization are indicated below the protein. (B) Proposed mechanism of action of O-antigen acetyltransferases during maturation of the LPS in the periplasm using OafA as an example. AT3, InterPro IPR002656; SGNH, InterPro IPR013830.

production of protective antibodies against *S.* Typhimurium infection (24, 27). Multiple *Salmonella* serovars have a rhamnose moiety in the O-antigen that can be acetylated at the 2- and 3-hydroxyl groups by F2GtrC proteins (9, 10, 23). As it is clear that F2GtrC is an acetyltransferase with no functional relationship to the GtrABC glycosylating proteins, we propose to rename this and orthologous rhamnose acetyltransferases OafB. The name reflects the protein architecture (O-antigen acetyltransferase-fused B), similar to what we suggest for OafA (O-antigen acetyltransferase-fused A).

In this work, using *in situ* and *in vitro* functional analysis of OafA and OafB O-antigen acetyltransferases, we address the following key questions to further our understanding of the mechanism of acetyl transport and transfer in AT3-SGNH fused acetyltransferases. (i) Are there essential residues in the membrane-bound AT3 domain that can give clues to their role in acetyl transfer? (ii) Can we obtain insight into the architecture of these proteins by elucidating the structure of the SGNH domain and its N-terminal extension? (iii) What is the function of the SGNH domain, and can it function independently of the AT3 domain?

RESULTS

***In silico* analysis identifies conserved features in the integral membrane domains of bacterial AT3 acetyltransferases.** The *S.* Typhimurium O-antigen acetyl-

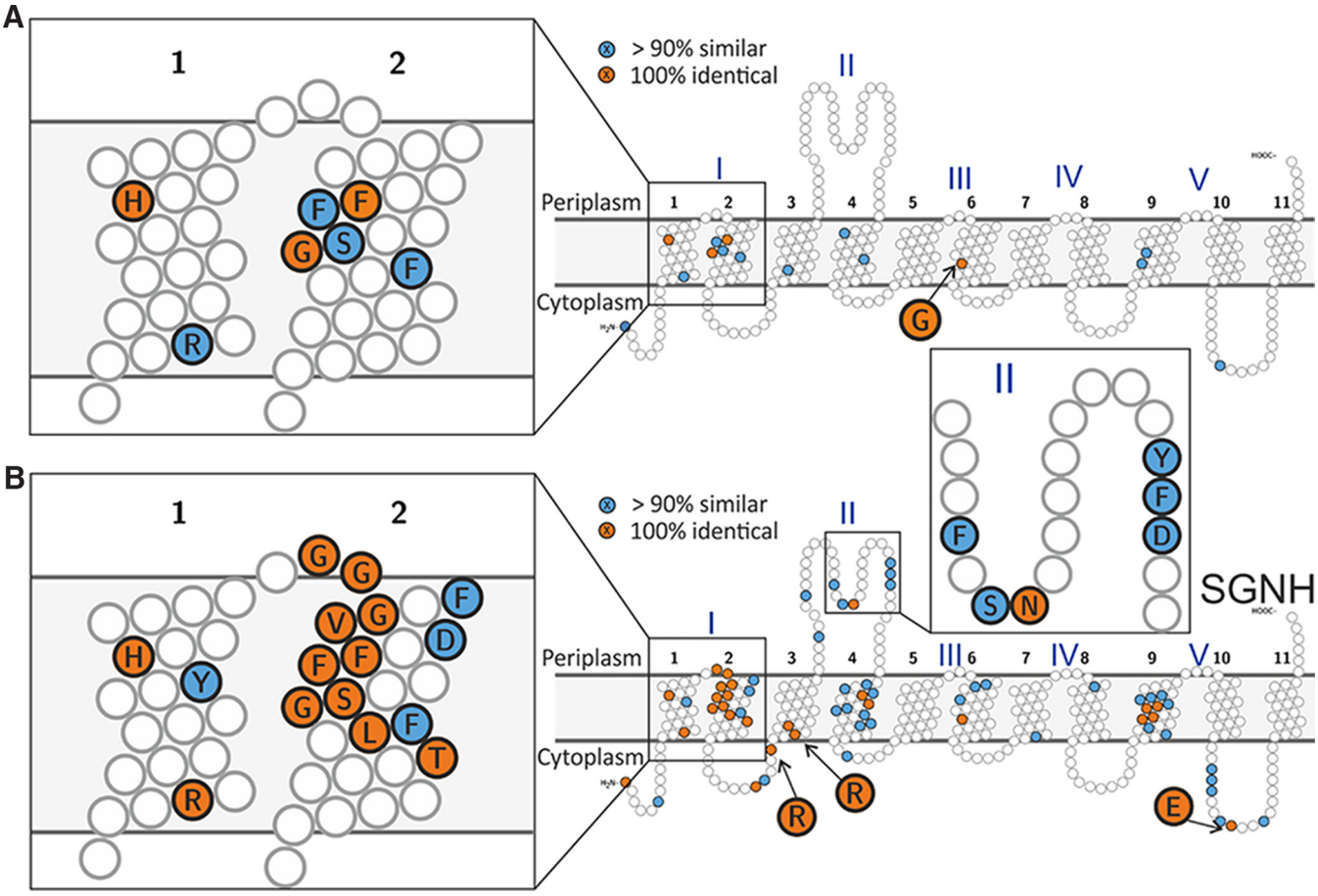

FIG 2 Conservation in transmembrane domains of experimentally characterized bacterial AT3 carbohydrate acetyltransferases. The 100% identical residues are colored orange, similar residues in >90% sequences are colored blue, and conserved small hydrophobic residues in transmembrane helices were not colored. (A) Conserved residues across all 30 currently known experimentally characterized proteins and OafB-SPA. (B) Conservation in only AT3-SGNH fused proteins in the alignment. See Table S1 for details of aligned sequences and Fig. S1 for full alignment.

transferases OafA (17) and OafB (23) (formerly F2GtrC) are both predicted by InterPro to contain an N-terminal AT3 domain (InterPro IPR002656, Pfam PF01757) fused to an SGNH domain (InterPro IPR013830, Pfam PF14606, or Pfam PF13472) (28, 29) (Fig. 1A). The AT3 domain has 10 TMH and an additional 11th helix that is presumably required to localize the fused SGNH domain in the periplasm (Fig. 1A) (30); this prediction is supported by experimental topology analysis of OafB (9) and consistent with topology analysis of Oac (31), a comparison enabled by our detailed alignments (see below). Reinforcing the widespread functions of these understudied proteins in bacteria, we identified in the literature 30 bacterial AT3 domain-containing proteins with experimentally confirmed carbohydrate acetyltransferase activity (9, 14–17, 32–55). Of these 30 proteins, 19 contain just the AT3 domain, while 11, including OafA and OafB, have the fused AT3-SGNH architecture (see Table S1 in the supplemental material). Previous work showed that in OafA and OafB, the SGNH domain is essential for acetyltransferase activity (9, 56), and thus, we propose the following working model for the mechanism of action (Fig. 1B). In AT3-SGNH proteins, the AT3 domain passes an acetyl group from an unidentified donor in the cytoplasm to the periplasmic face of the inner membrane. This acetyl group is then transferred to the SGNH domain, which catalyzes specific carbohydrate *O*-acetylation (Fig. 1B). To test this model, we first determined whether residues conserved between AT3-only and AT3-SGNH acetyltransferases are important for acetyltransferase activity.

Alignments of the 30 characterized AT3 acetyltransferases along with an *S. enterica* serovar Paratyphi A OafB homologue revealed that only 4 amino acids are invariant across all 31 proteins, $OafA_{H25}$, $OafA_{F41}$, $OafA_{G46}$, and $OafA_{G202}$ (Fig. 2A, Fig. S1). $OafA_{F41}$

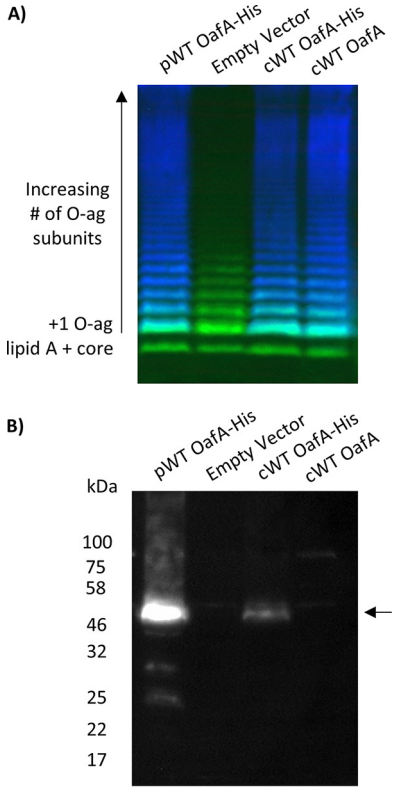

FIG 3 O-antigen acetylation and OafA expression from plasmid and chromosomally expressed protein. (A) LPS immunoblot with crude LPS extracts from *Salmonella enterica* serovar Typhimurium; LT2 basal O-antigen strain expressing OafA from pBADcLIC plasmid (pWT OafA-His), LT2 wild-type (WT) O-antigen strain with a C-terminal Deca-His tag added to the chromosomal copy of OafA (cWT OafA-His), the same strain with unmodified OafA (cWT OafA), and the LT2 basal O-antigen strain with an empty pBADcLIC plasmid (empty vector). O:5 antibody binding (blue) shows abequose acetylation, and *Salmonella* LPS core antibody binding (green) acts as a loading control. (B) Corresponding anti-His Western blot of insoluble protein fraction for detection of His-tagged OafA. The arrow indicates the full-length OafA protein.

and $OafA_{G46}$ belong to the FFXISG motif previously identified in unfused AT3 O-antigen acetyltransferases (Fig. S1) (31). Two conserved residues are predicted in TMH1, separated by 10 amino acids, in an R/K-X_{10}-H motif (Fig. 2A, Fig. S1). A previously identified RXXR motif ($OafA_{R69,R72}$) in loop 2-3 is essential for activity in *Shigella flexneri* Oac ($Oac_{R73,R75}$) (57) and OafB ($OafB_{R71,R73}$) (9). This motif is highly (but not absolutely) conserved across the 31 analyzed acetyltransferases.

We next examined features unique to the AT3 domains of AT3-SGNH fused acetyltransferases; these 11 sequences derive from diverse Gram-positive and Gram-negative bacteria (Fig. 2B, Table S1). The most striking shared feature of AT3-SGNH fused proteins is the highly conserved GG-F/Y-XGV-D/P/V motif located at the periplasmic side of TMH2 ($OafA_{G33\text{-}D39}$), which replaces a longer and more divergent loop region between TMH1-2 in the nonfused AT3 proteins. Further conserved residues are seen in the periplasmic loop between TMH3 and -4, including $OafA_{S112}$, $OafA_{N113}$, and $OafA_{Y122}$. Together, these observations suggest shared key residues in both AT3-only and AT3-SGNH fused proteins and possible adaption of AT3 domains in AT3-SGNH fused acetyltransferases toward their function together with the fused SGNH domain.

Site-directed mutagenesis combined with *in situ* functional analysis of OafA identifies functional residues within the AT3 domain. To determine the functional importance of conserved residues in *S.* Typhimurium OafA (OafA-STM), we developed an *in situ* functional assay using a double antibody LPS immunoblot. The assay quantifies both the level of acetylated abequose (O:5) and the amount of LPS based on the O-antigen core (Fig. 3). His-tagged OafA, or mutated versions thereof, were ex-

TABLE 1 Summary of site-directed mutagenesis analysis of the transmembrane domain of OafA[a]

Mutant	O:5 signal intensity compared to WT (% ± SEM)	Position	Reason for mutation
R14A	0.07 ± 0.04	TMH1	Specifically conserved in AT3-SGNH proteins
H25A	0.33 ± 0.18	TMH1	Conserved in TMH1 across all aligned proteins
S32A	105.25 ± 30.89	Periplasmic loop and TMH2	XGG-F/Y-XGV-D/P/V-X motif found to be conserved in AT3-SGNH fused acyltransferases. In the first periplasmic loop between TMH1-2
G33A	119.17 ± 18.72	Periplasmic loop and TMH2	
G34A	1.36 ± 0.88[b]	Periplasmic loop and TMH2	
F35A	19.24 ± 2.70	Periplasmic loop and TMH2	
I36A	101.47 ± 22.72	Periplasmic loop and TMH2	
G37A	118.13 ± 22.11	Periplasmic loop and TMH2	
V38A	86.38 ± 12.73	Periplasmic loop and TMH2	
D39A	0.31 ± 0.07	Periplasmic loop and TMH2	
V40A	121.28 ± 23.82	Periplasmic loop and TMH2	
S45A	98.18 ± 24.30	TMH2	Conserved in SG in TMH2
G46A	99.59 ± 22.01	TMH2	
R69A	0.10 ± 0.04	TMH3	RXXR motif previously identified as critical for function
R72A	0.07 ± 0.02	TMH3	
S112A	0.24 ± 0.09	TMH3-4 Periplasmic loop	Conserved in periplasmic loop between TMH3-4 in AT3-SGNH fused proteins
N113A	93.79 ± 14.92	TMH3-4 Periplasmic loop	
Y122A	85.76 ± 7.58	TMH3-4 Periplasmic loop	
G202A	74.14 ± 10.70	TMH6	Conserved transmembrane glycine
E325A (linker)	4.84 ± 1.13	TMH10-11 cytoplasmic loop	Conserved after TMH10 in all AT3-SGNH fused proteins

[a]Dark gray shading, point mutants with <1% O:5 signal intensity; Light gray shading, point mutants with <50% O:5 signal intensity.
[b]No OafA protein expression detected. Values represent the average of 2 biological repeats with 3 technical replicates.

pressed in *trans* in a strain that lacks all O-antigen modification genes, including *oafA* (strain 293) (see Materials and Methods; Table S2). Levels of abequose acetylation in these strains were determined with LPS immunoblotting from the signal obtained with serotype antibody, and protein expression was also confirmed (Fig. 3, Fig. S2). We validated this approach by comparing abequose acetylation to both chromosomal His-tagged OafA and wild-type OafA using the in *trans* system. This showed that

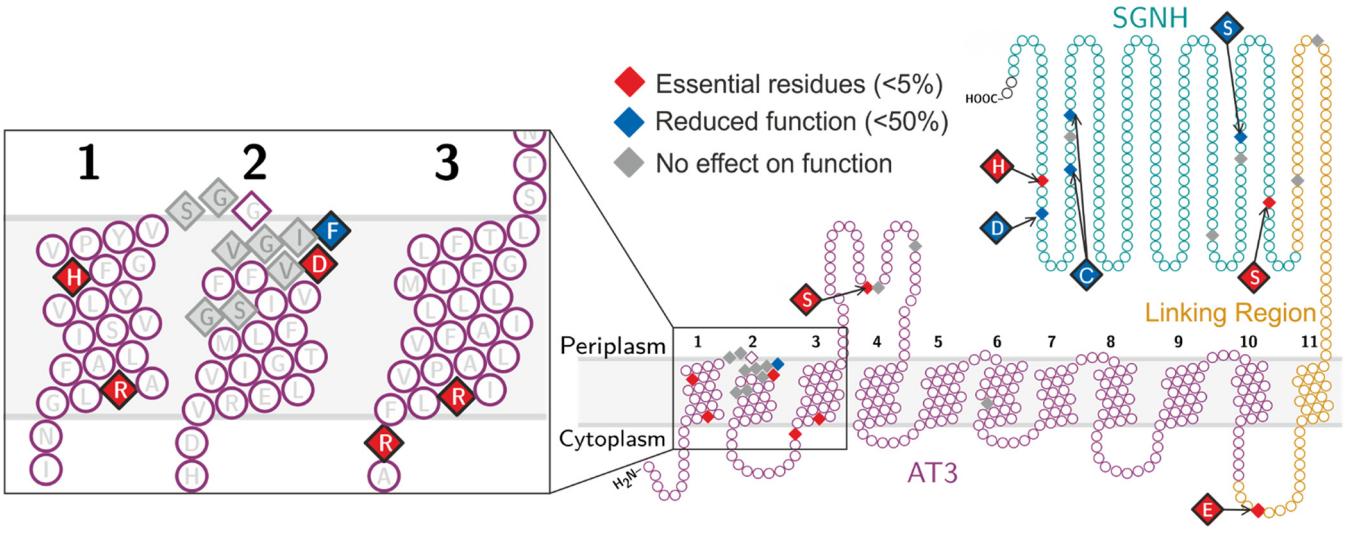

FIG 4 Summary of mutagenesis analysis of *S.* Typhimurium OafA. A diamond shape indicates residues that were mutated, cysteine residues were mutated to serine, and all other residues were mutated to alanine. Results relate to the percentage O-antigen acetylation compared to the wild type; mutants that caused loss of protein expression are diamond shaped but not colored (G34A).

despite a higher level of protein in the in *trans* system (Fig. 3B), a comparable level of abequose acetylation was obtained in all strains (Fig. 3A, Fig. S2).

Twenty positions in the membrane-bound domain of OafA were individually engineered to replace the wild-type amino acid with alanine. The level of O-antigen acetylation *in situ* as a result of mutant protein expression is summarized in Table 1 and Fig. 4, and the data are shown in Fig. S2. Point mutants that gave <1% O-antigen acetylation signal in relation to the wild type were considered to be inactive, and those with <50% O-antigen acetylation signal were considered to have significantly reduced activity. For all mutant proteins except G34A, there was detectable full-length protein on the Western blot, sometimes in addition to degradation products (Fig. S2). Assay validation experiments indicate that the levels of full-length mutant protein are in excess of wild-type levels and thus should be sufficient to confer detectable abequose *O*-acetylation.

The arginine and histidine residues in the R/K-X_{10}-H motif ($OafA_{R14}$ and $OafA_{H25}$) are essential for function. These residues are predicted to be on the same surface of the alpha helix with spacing similar to the predicted distance between the 3′ phosphate and the thioester bond of one coenzyme A molecule (~19 Å). Thus, we hypothesize that these residues provide a potential acetyl-CoA interaction site within the AT3 domain. The 100% conserved glycines ($OafA_{G46}$ and $OafA_{G202}$) could be replaced with alanine with no detriment. As expected, both arginines in the TMH3 RXXR motif ($OafA_{R69,R72}$) (9, 57) were essential for OafA function (Table 1, Fig. 4).

We next examined the unique aspects of the AT3 domains among the AT3-SGNH fused proteins. Of the conserved GG-F/Y-XGV-D/P/V motif and flanking residues, mutation of $OafA_{F35}$ and $OafA_{D39}$ caused significant reduction and complete loss of OafA activity, respectively. $OafA_{S112A}$ mutation also caused complete loss of OafA activity (Table 1, Fig. 4). AT3-only acetyltransferases do not contain an 11th TMH, but a glutamate residue after the C-terminal end of TMH10 ($OafA_{E325}$) is invariant across AT3-SGNH protein sequences; mutation of this residue ($OafA_{E325A}$) resulted in significant reduction in OafA activity (Table 1, Fig. 4). Thus, AT3-SGNH-specific conserved residues in the AT3 domain are inherently involved in the mechanism of action of OafA.

OafB-SPA^{long} has an extended SGNH-like fold. To gain an understanding of the mechanism of OafA and OafB, both domains must be analyzed; thus, *in vitro* analysis of the SGNH domain was conducted. Structural analysis of the SGNH domains and periplasmic linking regions of OafA and OafB were used to gain insight into the functional adaptations of an SGNH domain fused directly to an AT3 domain. We expressed and purified residues 366 to 609 from OafA (OafA-STM$^{C\text{-}long}$) and residues 377 to 640 from *S.* Paratyphi OafB (OafB-SPA$^{C\text{-}long}$), which have 31% sequence identity (Fig. 1A). Although OafB-SPA has not been experimentally characterized in the literature, *S.* Paratyphi O-antigen rhamnose can be acetylated (58), and OafB-SPA has 78% sequence identity to the experimentally characterized OafB-STM rhamnose acetyltransferase (9).

No diffracting crystals of OafA-STM$^{C\text{-}long}$ were obtained; however, crystals diffracting to a 1.1-Å resolution were obtained for OafB-SPA$^{C\text{-}long}$, with a single molecule in the asymmetric unit. The structure could not be solved by molecular replacement using a number of known SGNH structures but was solved using Fragon (59) with a 14-residue ideal polyalanine α-helix as the search model and refined to an R_{work}/R_{free} of 13.6/14.9% (Table S3).

The core structure of OafB-SPA$^{C\text{-}long}$ resembles an SGNH domain with an $\alpha/\beta/\alpha$ hydrolase fold consisting of five central β-strands surrounded by six α-helices (Fig. 5A). Two disulfide bonds are seen in the structure (Fig. 5A) and were verified using mass spectrometry. The closest structural homologues to OafB-SPA$^{C\text{-}long}$, as identified by the DALI server, are carbohydrate esterases from *Talaromyces cellulolyticus* (Protein Data Bank [PDB] 5B5S) and *Clostridium thermocellum* (PDB 2VPT); each has a root mean square deviation (RMSD) of 2.5 Å over 207 and 201 backbone residues, respectively.

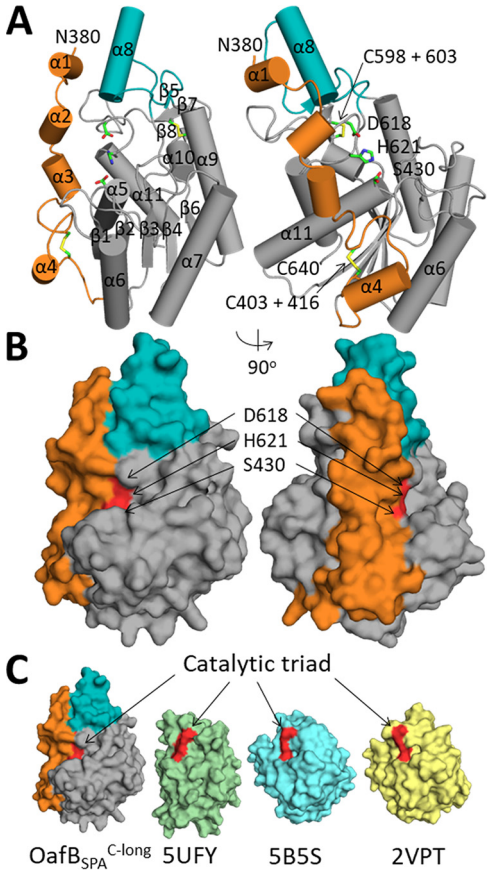

FIG 5 Analysis of the crystal structure of OafB-SPA$^{C\text{-}long}$. (A) Cartoon representation of OafB-SPA$^{C\text{-}long}$ with helices and sheets numbered, with the additional helix (α8) colored teal and SGNH-extension colored orange. Catalytic residues and disulfide bonds are shown as sticks and are labeled. (B) Surface representation of OafB-SPA$^{C\text{-}long}$ with coloring as above and the catalytic triad colored red. (C) Surface representation of OafB-SPA^{long}, PDB 5UFY, PDB 5B5S, and PDB 2VPT.

The first clear difference between OafB-SPA$^{C\text{-}long}$ compared to its closest structural homologues and the only other SGNH domain from a fused acyltransferase with a solved crystal structure, OatA-SGNH (PDB 5UFY) (60), is that the structure is significantly larger, at ~36,000 Å^3, than OatA-SGNH at ~23,000 Å^3, which is more similar to the size of the two most closely related structures of the carbohydrate esterases (PDB 2VPT is ~26,000 Å3 and PDB 5B5S is 27,000 Å3). This additional volume in the fold is contributed by two separate noncontiguous parts of the structure, the first being helix α8, which comprises 10% of the SGNH domain volume (Fig. 5). A structure-based alignment of related SGNH domains indicated that the sequence forming this additional helix is only present in AT3-SGNH domains involved in acetylation of LPS O-antigens (Fig. 6A, Fig. S3) and so is missing on OatA. Second, and most significantly, the region that connects the end of TM11 and the start of the sequence of other known SGNH domains (residues 377 to 421) is clearly structured and forms a long extension of the SGNH domain that we now term the SGNH extension (SGNH$_{ext}$). The SGNH$_{ext}$ interacts extensively with the SGNH domain covering 1,500 Å^2 of the SGNH domain, including interactions with helix α8; 38 amino acids of the SGNH domain interact with 32 (of 48) residues in the extension. Removal of the most N-terminal half of the SGNH$_{ext}$ (OafA-STM$^{C\text{-}short}$ and OafB-SPA$^{C\text{-}short}$ [Fig. 1A]), results in a decrease in melting temperature of 5.7°C in OafA and 8.9°C in OafB, suggesting that the SGNH$_{ext}$ has a stabilizing effect on the SGNH domain (Fig. S4). These observations show that OafB-SPA$^{C\text{-}long}$ forms an extended SGNH-like fold with an additional helix, and the periplasmic portion of the linking region is structured and interacts with the SGNH domain.

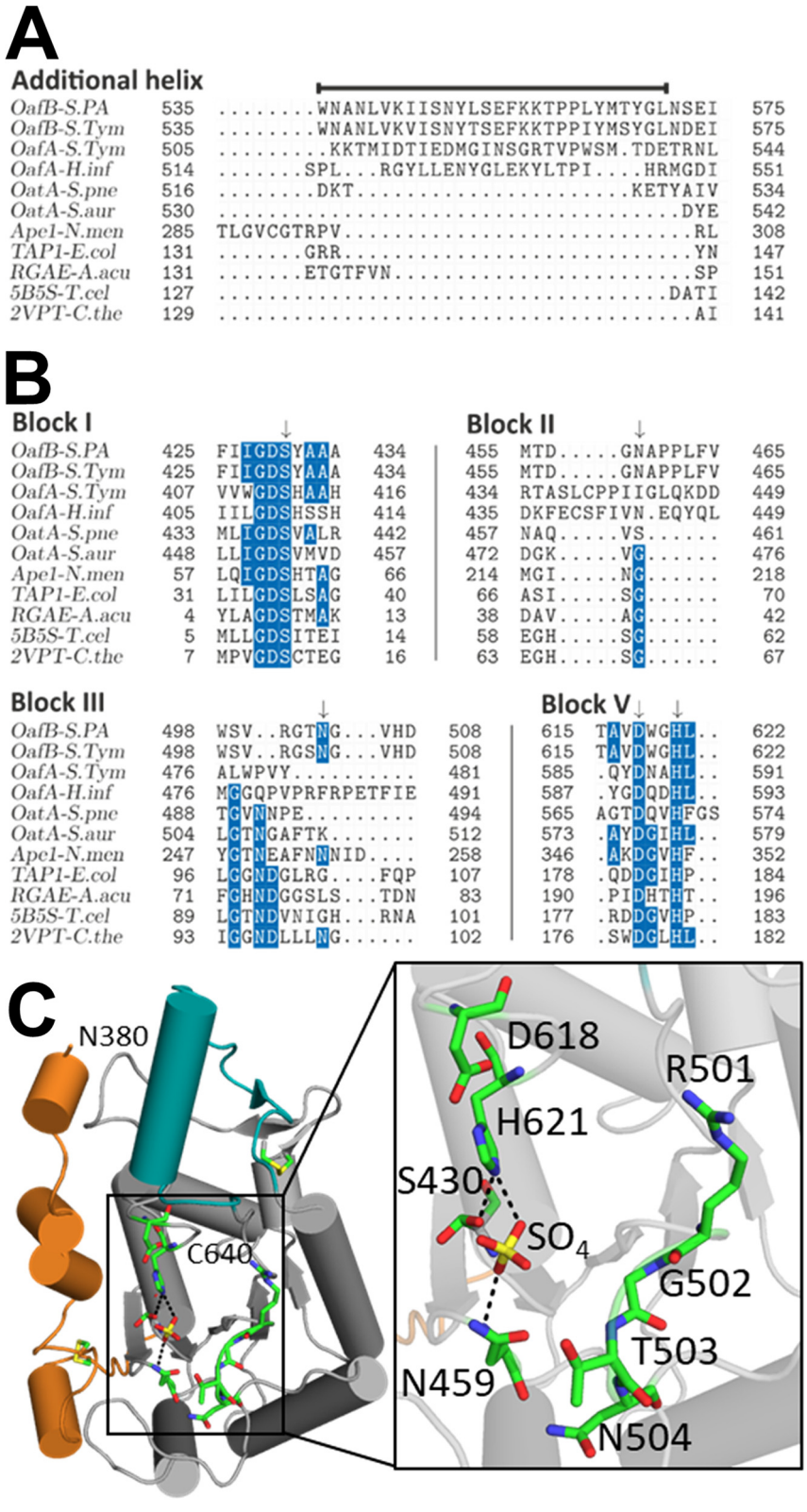

FIG 6 Analysis of additional helix and catalytic triad residues (A and B) Structure-based sequence alignments of additional helix (A), indicated by a line above the sequence, and blocks I to V (B) with residues conserved in >50% of sequences highlighted blue; catalytic and oxyanion hole residues are indicated by an arrow. Abbreviations and details of sequences used are in Materials and Methods. (C) Catalytic triad and potential oxyanion hole residues are shown as sticks; hydrogen bonds to cocrystallized sulfate ion are shown as dotted black lines.

TABLE 2 Summary of site-directed mutagenesis analysis of the periplasmic domain of OafA[a]

Mutant	O:5 signal intensity compared to WT (% ± SEM)	Reason for mutation
C383,397S (linker)	107.40 ± 26.80	Conserved disulfide bonding pairs
C439,453S	185.06 ± 54.63	Conserved disulfide bonding pairs
C567,572S	49.98 ± 4.33	Conserved disulfide bonding pairs
S437A	45.59 ± 3.42	Potential oxyanion hole residue
E569A	99.87 ± 7.01	Conserved between most C-term Cys pair
S412A	0.36 ± 0.26	SGNH domain catalytic triad residues
D587A	10.13 ± 1.70	SGNH domain catalytic triad residues
H590A	0.87 ± 0.62	SGNH domain catalytic triad residues

[a]Dark gray, point mutants with <1% O:5 signal intensity; light gray, point mutants with <50% O:5 signal intensity. Values represent the average of 2 biological repeats with 3 technical replicates.

Catalytic residues of OafB-SPA^{long} resemble a typical SGNH domain with an atypical oxyanion hole. SGNH domains are usually characterized by the presence of four blocks of sequence containing conserved residues, block I (GDS), block II (G), block III (GxND), and block V (DxxH) (where x is any nonproline residue) (22). The structure-based sequence alignment was used to identify conserved residues in the SGNH domain of fused acyltransferases (Fig. 6B, Fig. S3). The typical SGNH catalytic triad, consisting of serine (block I), aspartic acid, and histidine (block V), is conserved in the sequence of both OafA and OafB. *In situ* functional analysis of catalytic triad mutants OafA$_{S412A}$ and OafA$_{H590A}$ showed almost complete loss of function, whereas OafA$_{D587A}$ showed reduced activity (Table 2, Fig. S2). This is consistent with analyses of typical catalytic triad activity in other SGNH proteins (61, 62).

While the catalytic triad is conserved in both proteins, the oxyanion hole residues, glycine (block II) and asparagine (block III), are not (Fig. 6B). Analysis of the structure-based alignment of the block II region (Fig. 6B, Fig. S3) reveals that the conserved glycine is replaced by an asparagine in OafB (OafB$_{N459}$). The structure of OafB-SPA$^{C\text{-}long}$ shows OafB$_{N459}$ to be within hydrogen-bonding distance of a cocrystallized sulfate ion (Fig. 6C), suggesting that OafB$_{N459}$ could interact with bound substrate and participate in oxyanion hole formation. Homology modeling of OafA-STM$^{C\text{-}long}$ based on the structure of OafB-SPA$^{C\text{-}long}$ (Fig. S5) suggests that the OafA$_{S437}$ side chain or OafA$_{L438}$ is most likely to replace the block II glycine in the oxyanion hole. This was supported by the *in situ* abequose acetylation assay, which shows that OafA$_{S437A}$ has significantly reduced activity in comparison to wild-type OafA (Table 2, Fig. S2), consistent with the decrease in activity seen on mutation of the oxyanion hole residues in other SGNH domains (60, 61, 63).

The GxND motif (block III), where Asn is typically involved in oxyanion hole formation (20), is not evident in OafA or OafB in the structure-based alignment (Fig. 6B). OafB-SPA$^{C\text{-}long}$ contains a GTNG motif (OafB$_{G502\text{-}G505}$) close to sequence block III (Fig. 6B), but the side chains of these residues are oriented away from the catalytic triad (Fig. 6C). These observations suggest that, although OafA and OafB display the typical catalytic triad of an SGNH domain, their oxyanion hole arrangement is atypical.

The SGNH$_{ext}$ confers acceptor specificity. The structured region that extends the OafB SGNH domain (SGNH$_{ext}$) appears to occlude the active site and results in significantly lower solvent-accessible surface area (SASA) of the catalytic triad residues (40 Å) than in OatA, 2VPT, and 5B5S (132 Å, 110 Å, and 126 Å, respectively) (Fig. 5C). Removing the 22 most N-terminal residues from the structure of OafB-SPA$^{C\text{-}long}$ (OafB-SPA$^{C\text{-}short}$; Fig. 1A) increases the SASA of the catalytic triad residues of OafB to 107.9 Å.

To assess the potential consequences of an occluded active site for substrate specificity, assays were carried out for OafA and OafB containing the full SGNH$_{ext}$ (OafA-STM$^{C\text{-}long}$ and OafB-SPA$^{C\text{-}long}$) and those with half the SGNH$_{ext}$ (OafA-STM$^{C\text{-}short}$ and OafB-SPA$^{C\text{-}short}$) (Fig. 1A). *In vitro* catalytic activity was first confirmed for all constructs via their ability to hydrolyze the ester substrate p-nitrophenyl acetate

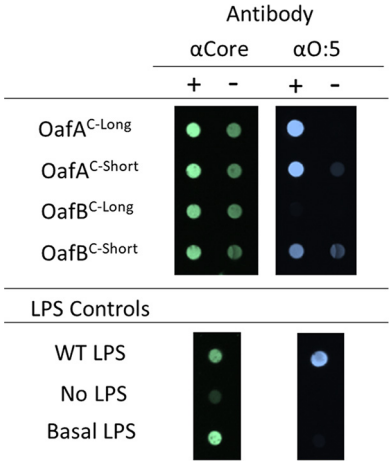

FIG 7 Effect of $SGNH_{ext}$ length on substrate specificity of C-terminal OafA and OafB. Dot blot for acetylated abequose (αO:5, blue) on basal *Salmonella enterica* serovar Typhimurium LPS after incubation with purified C-terminal OafA and OafB and pNPA as an acetyl group donor; 10 μM OafA and 20 μM OafB were used in these reactions. αCore antibody (green) was used as a loading control. WT acetylated LPS was used as a positive control. +, Active protein; –, heat-treated protein. Representative of $n = 3$ repeats. "C-long" constructs comprise the SGNH domain with full $SGNH_{ext}$, "C-short" constructs comprise the SGNH domain with fewer $SGNH_{ext}$ residues to expose the SGNH domain active site. See Fig. 1 for details of the C-terminal OafA and OafB constructs.

(pNP-Ac) (Fig. S6), an assay commonly used to test SGNH domain function (64, 65). This activity suggests that all four proteins are correctly folded and catalytically active regardless of the presence or absence of the $SGNH_{ext}$ residues covering the active site (Fig. S6).

To assess whether $SGNH_{ext}$ affects the *in vitro* acceptor substrate specificity of OafA-$STM^{C\text{-}term}$ and OafB-$SPA^{C\text{-}term}$ proteins, purified proteins were incubated with pNP-Ac (acetyl group donor) and unmodified *S.* Typhimurium LPS (Path993; Table S2) as the acceptor substrate, and O:5 antibodies were used to probe for O-antigen abequose acetylation. Abequose is the native acceptor sugar for OafA, whereas OafB acetylates rhamnose *in situ*. A positive signal for O:5 antibody binding is gained after incubation with OafA-$STM^{C\text{-}long}$ and OafA-$STM^{C\text{-}short}$ (Fig. 7). Thus, OafA-$STM^{C\text{-}long}$ and OafA-$STM^{C\text{-}short}$ are able to acetylate their native substrate in solution. In contrast, acetylation of the nonnative acceptor substrate by OafB occurs only in the absence of the OafB $SGNH_{ext}$ (OafB-$SPA^{C\text{-}short}$) (Fig. 7). First, these results support our working model that the SGNH domain performs the last step in the transferase reaction, the transfer of the acetyl moiety to the acceptor carbohydrate. Furthermore, these results strongly indicate that the acceptor substrate specificity of this SGNH domain is constrained by the cognate, structured $SGNH_{ext}$.

Evolutionary support for an interaction between the AT3 domain and the SGNH domain. The discovery that the "linker" region that is present between the more clearly defined AT3 and SGNH domains is, in fact, a long structured component of the SGNH domain means that the SGNH is much more constrained and proximal to the membrane than initially proposed if this region was a long flexible linker. The discovery that there are residues in the AT3 loop between TMH3 and -4 that are only conserved in the AT3-SGNH fused proteins suggests potential protein-protein contacts between the two domains during catalysis. To test this hypothesis, we used a coevolution analysis of the OafA-B type acetyltransferases to assess whether there was any evidence for correlated changes in the two domains consistent with a physiological interaction (Fig. S7a). While there are many correlated changes within the two separate domains, a significant correlated change was observed between residues 95 and 97, located in the periplasmic loop between TMH3 and -4 of the AT3 domain (Fig. 8) and residues 542 and 545 to 546, which form a surface-accessible patch (Fig. S7b) on the additional helix

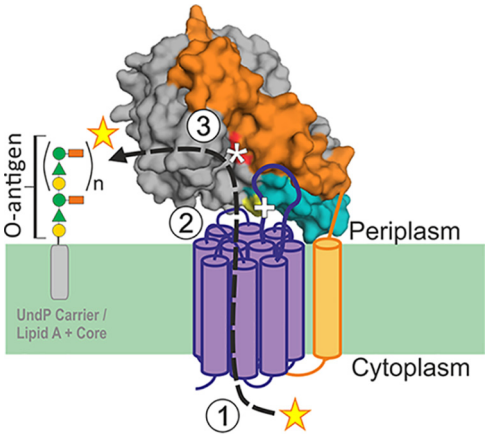

FIG 8 Refined model of AT3-SGNH fused O-antigen acetyltransferases. Periplasmic $SGNH_{ext}$ (orange) is structured, therefore positioning the SGNH domain (gray) close to the AT3 domain (purple); this orients the additional helix (teal) in close proximity to the AT3 domain with interactions between the two domains as proposed by the coevolution analysis. These observations result in the current hypothesis: (1) Cytoplasmic acetyl group donor interacts with conserved Arg in TMH1, the acetyl group is processed and transferred to the periplasmic side of the inner membrane, and this process involves catalytic His residue of TMH1. (2) Conserved Asp and Ser mediate transfer of acetate to the SGNH domain. (3) SGNH domain catalyzes addition of the acetate to specific O-antigen monosaccharide. The active site of the SGNH domain is highlighted by an asterisk, and interaction site is highlighted by a plus sign (+).

(α8) of the SGNH domain (Fig. 8). This predicted interaction further informs our refined topological model of these AT3-SGNH acetyltransferases (Fig. 8).

DISCUSSION

AT3 domain-containing proteins (PF01757) are a ubiquitous family of proteins involved in diverse carbohydrate modifications across the domains of life. Prokaryotic members of this family play roles in modification of antibiotics and antitumor drugs, as well as initiation of microbial symbioses with plants (15, 66, 67) (Table S1). In bacterial pathogens, such as *Salmonella enterica*, *Listeria monocytogenes*, *Haemophilus influenzae*, and *Streptococcus pneumoniae*, these proteins are implicated in acetylation of extracytoplasmic polysaccharides, which can have significance for interactions with phage and hosts and can affect virulence and antibiotic resistance (24, 32, 36, 38). The current experimentally characterized AT3 domain-containing carbohydrate *O*-acetyltransferases display SGNH-fused or AT3-only domain architecture. Although both AT3 and SGNH domains display broad substrate ranges in diverse biological systems, the mechanism of action of both SGNH-fused and AT3-only acetyltransferases is largely unknown.

Previous understanding of AT3-SGNH fused acetyltransferases was obtained by *in situ* functional assays and structure-function assessment of the SGNH domain (9, 17, 60). Here, expanded bioinformatic analysis with a set of 30 experimentally characterized bacterial AT3 acetyltransferases, including AT3-only and AT3-SGNH fused protein sequences, which perform a range of biological functions (Table S1), revealed commonalities and key differences. For example, an R/K-X_{10}-H motif in TMH1 is shared across all the bacterial AT3 acetyltransferases studied (Fig. 2) and is also highly conserved across all AT3 domain proteins in the Pfam database (29), strongly suggesting that these are critical catalytic residues relevant to the whole protein family.

$OafA_{R14}$ and $OafA_{H25}$ within this motif were essential for activity (Table 1, Fig. 4) and are predicted to be at opposite ends, but on the same surface, of the TMH1 helix (arginine toward the cytoplasmic side), providing a potential interaction site for the proposed acetyl group donor acetyl-CoA. Although cytoplasmic acetyl-CoA has not been confirmed as the donor for O-antigen acetylation, it occupies a central role in bacterial metabolism and is a prominent source of acetate in bacterial cells (68, 69). Arginine residues were implicated in binding of the 3′ phosphate of acetyl-CoA in other

acetyltransferase proteins (70), and conserved histidine residues in the soluble mitochondrial carnitine O-acyltransferase coordinate the thioester bond of acyl-CoA with the carnitine acceptor to catalyze the acyl-transfer reaction (71). Significantly, the equivalent residue was discovered as a natural histidine to tyrosine point mutation that decreased function of the *Streptococcus pneumoniae* capsule acetylation protein WcjE in clinical isolates (72).

A similar role for a conserved intermembrane histidine residue has also been suggested for membrane-bound O-acyltransferases containing an MBOAT (InterPro IPR004299) rather than AT3 domain (73). These observations support a role of the R/K-X_{10}H motif in coordinating a cytoplasm-derived acetyl-CoA molecule within the membrane-bound AT3 domain for transfer of the acetyl group to the SGNH domain, consistent with our model (Fig. 1). AT3 domain-containing proteins are implicated in transferring a wide range of acyl groups such as succinate, isovalerate, and propionate (67, 74, 75); these can all be carried by coenzyme-A. The proposed mechanism of acetyl donor interaction would provide a potential conserved mechanism for transfer of any of these acyl substituents, supporting the idea that the TMH1 arginine and histidine are fundamentally important for the mechanism of all AT3 domain-containing acyltransferases.

Residues specifically conserved in the AT3 domains of AT3-SGNH fused proteins ($OafA_{F35}$ and $OafA_{D39}$ in TMH2 and $OafA_{S112}$ between TMH3 and -4) are located toward the periplasmic side of the AT3 domain (Fig. 2); we suggest these are likely to be important for interaction with the O-antigen substrate or SGNH domain for acetyl group transfer. In contrast to the essential nature of $OafA_{S112}$ in the periplasmic loop between TMH3 and -4, no functional residues have been identified in the equivalent region of *S. flexneri* Oac (an AT3-only O-antigen acetyltransferase) (57). Conversely, the invariant glycine residue $OafA_{G46}$, which was critical in *S. flexneri* Oac (Oac_{G53}) (Fig. S1) (31, 57), could be replaced by alanine without affecting the function of OafA. These observations suggest a divergence between AT3-only and AT3-SGNH fused proteins. The location of critical residues specific to the AT3-SGNH fused proteins further suggest that this divergence occurs at the point of acetyl group transfer to the acceptor substrate.

This study demonstrates that the SGNH domain of OafA is able to acetylate the abequose of the O-antigen of *Salmonella in vitro* without the presence of its cognate fused AT3 domain. This supports the predicted role for SGNH in the final step of acetyl group transfer to the acceptor substrate in fused acetyltransferases (Fig. 1B). In agreement with this, in the two-component PatA/PatB peptidoglycan acetyltransferase system, PatB, a soluble SGNH protein, is responsible for transfer of the acetyl group onto the peptidoglycan substrate (62). Moynihan and Clarke hypothesized that PatA (an MBOAT protein, not an AT3) is responsible for transporting the acetyl group across the membrane, where it is transferred to the acceptor by the soluble PatB protein (62). The membrane-bound PatA MBOAT protein in this system is interchangeable with WecH, an AT3-only acetyltransferase protein (52, 76), giving an example of direct transfer of acetate between a membrane-bound AT3 domain and soluble SGNH domain protein. This supports the mechanistic model of the AT3 domain delivering the acetyl group to the SGNH domain for transfer onto the acceptor substrate in AT3-SGNH fused proteins (Fig. 1B).

Our data demonstrated, for the first time in a fused system, the necessity for the fused SGNH domain in glycan carbohydrate acetylation. However, this poses the conundrum that other closely related systems, such as OacA from *Shigella*, which *O*-acetylates rhamnose in the O-antigen (57), lack either a fused or genetically linked partner SGNH domain. Consequently, either the AT3 domain functions differently or there is a currently undiscovered partner protein.

This study elucidates the structure of the $SGNH_{ext}$ in OafB-$SPA^{C\text{-}long}$ and shows that removal of this region results in promiscuity of carbohydrate modification in *in vitro* acetyltransferase reactions (Fig. 7). These findings suggest that the $SGNH_{ext}$ plays a role in determining the specificity of the O-antigen residue to be acetylated. Closer exam-

ination of the structure reveals that two tyrosines, Tyr289 and Tyr394, in the $SGNH_{ext}$ sit close to the active site and could potentially be involved in a mechanism to limit off-target acetylation. Inadvertent acetylation of complex carbohydrates could potentially have diverse and undesired biological effects due to the variation of cellular processes that can be affected by acetylation (9, 33, 39, 77–79). Whether this also suggests that AT3 proteins all need a partner domain or protein for substrate-specific transferase activity remains to be determined.

Coevolution analysis predicts interaction between periplasmic loops of the AT3 domain and the SGNH domain of OafB. This is similar to the arrangement of domains seen in PglB, an oligosaccharide transferase from *Campylobacter lari* (80), with 13 TMH and a periplasmic domain. In PglB the periplasmic domain interacts via periplasmic loops in the transmembrane domain, and both domains are hypothesized to interact with the peptide substrate (80). In our model, the coevolution analysis positions the periplasmic loops of the AT3 domain close to the α8 helix in the SGNH domain, allowing for an interaction with each other and with the acceptor substrate (Fig. 8).

AT3 domain-containing proteins are involved in the modification of a wide range of polysaccharides and influence many host-pathogen interactions. These structural and functional insights can be applied to the well-studied and biotechnologically relevant AT3 proteins, including Nod factor modifications important for plant microbe symbiosis, and antitumor and antibiotic modifying proteins. Furthermore, this work can inform future studies of eukaryotic systems where AT3 domain-containing proteins are involved in regulation of the life span of *Caenorhabditis elegans* (81) and in *Drosophila* development (82).

MATERIALS AND METHODS

Bacterial strains, plasmids, and culture conditions. *Escherichia coli* and *S.* Typhimurium strains and plasmids are listed in Table S2. Strains were cultured in Lennox broth (LB; Fisher Scientific) at 37°C with appropriate antibiotic selection unless otherwise stated.

***In silico* analysis of bacterial AT3 domains to identify conserved residues.** A survey of the literature identified 30 experimentally characterized bacterial carbohydrate acetyltransferases; these sequences were aligned with OafB from *S.* Paratyphi A, using T-coffee (83). Protein accession numbers are in Fig. S1. T-coffee was also used to align the OafA-STM, OafB-STM, and OafB-SPA protein sequences for direct comparison.

Structure-based sequence alignments using PROMALS3D with default settings were carried out with the two closest structural homologues identified using the DALI server and a selection of typical SGNH domains for which structural information is available, OafB-SPA, 1IVN, 4K40, 1DEX, 5UFY, 5B5S, and 2VPT. Five additional representative sequences of OafA, OafB, and OatA were included (A0A0H2WM30, STMMW_03911, Q8ZNJ3, NTHI0512, and Q2FV54).

Coevolution analysis. A multiple sequence alignment of AT3 SGNH domain fused proteins was constructed using the MUSCLE alignment tool based on 1,188 full-length sequences from the UniProt reference proteomes. This alignment was used to construct a profile hidden Markov model (HMM) to detect further homologues in the UniProt reference proteome set as well as within the MGnify protein sequence set. We required that all matches to this profile-HMM had a sequence and domain threshold of 27 bits. We also required that the sequence matched >90% of the HMM match states to ensure that homologues with only one of the two domains were not included in the alignment.

A total of 2,713 homologues were identified from the UniProt reference proteome set, and 9,757 homologues were identified from the MGnify metagenomics sequences. A large sequence alignment was constructed using OafB as the master with no indels with all the sequence matches aligned to it using the hmmalign package and a custom Perl script to format the alignment for contact prediction. The alignment was submitted to the RaptorX contact prediction server (84).

Molecular biology. Primers (Sigma-Aldrich) are listed in Table S2. Mutations were introduced into the OafA sequence (pMV433 as the template), which had been cloned into pBADcLIC using blunt-end ligation, placing the gene under the control of an arabinose-inducible promoter. Mutants were confirmed by sequencing. Plasmids were electroporated into *S.* Typhimurium strain 293 (Table S2) for analysis of activity.

All *oafA*-STM and *oafB*-SPA sequences for protein expression were cloned into pETFPP_2 (Technology Facility, University of York) using in-fusion cloning (Clontech) to add a 3C-protease cleavable N-terminal His-MBP tag. Plasmid pMV433 (Table S2) was used as the template for creation of expression plasmids encoding the protein sequence for OafA-$STM^{C\text{-}long}$ (residues 366 to 609) and OafA-$STM^{C\text{-}short}$ (residues 379 to 609). *oafB*-SPA (UniProt A0A0H2WM30), amino acid residues 377 to 640 for OafB-$SPA^{C\text{-}long}$, was codon-optimized for *E. coli* and synthesized by Genewiz in a pUC57-Kan vector. This vector was then used as a template for the sequence encoding OafB-$SPA^{C\text{-}short}$ (residues 399 to 640); see Table S2 for the primers used.

***In situ* functional analysis of OafA variants.** All *in situ* functional analyses of OafA variants cloned into pBADcLIC were carried out in strain Path293 (23) (Table S2). Strains for the *in situ* functional analysis were cultured at pH 7.0 in 100 mM sodium phosphate-buffered LB at 37°C in a baffled conical flask with shaking at 200 rpm. Overnight cultures were diluted 100-fold and grown for 16 h. Samples were normalized to an optical density at 600 nm (OD_{600}) of 3.0 per ml for LPS and protein extraction.

Crude LPS sample preparation. The method was adapted from Davies et al. (23). First, 1 ml of OD-normalized (OD_{600}, 3.0) overnight culture was pelleted for 5 min at 16,000 × *g*. Cell pellets were resuspended in 100 μl LPS sample buffer (60 mM Tris-HCl, 1 mM EDTA, pH 6.8) containing 2% (wt/vol) SDS and then boiled at 100°C for 5 min. Then, 400 μl of LPS buffer was used to dilute the solution before RNase (Roche) and DNase (Sigma) treatment at 37°C for 16 h. Samples were then treated with 100 μg proteinase K for 16 h at 50°C, and 7.5 μl of crude LPS extracts were run on 1.0 mm Tricine SDS poly acrylamide gel electrophoresis (TSDS-PAGE gel) for analysis by immunoblotting.

Detection of OafA protein expression for *in situ* assays. First, 1 ml of OD-normalized culture was pelleted for 5 min at 16,000 × *g*. Soluble and insoluble fractions were isolated from cell pellets using BugBuster solution (Novagen) following the manufacturer's instructions for soluble protein extraction. The insoluble pellet was resuspended in 75 μl of sample buffer (10% [vol/vol] glycerol, 1% [wt/vol] SDS, 10 mM Tris-HCl [pH 7.2], 0.06% [wt/vol] bromophenol blue, 3% [vol/vol] β-mercaptoethanol), heated to 60°C for 10 min, and centrifuged for 10 min at 16,000 × *g*. Then, 10 μl of insoluble fraction samples was loaded onto a 12% acrylamide 1.0-mm SDS-PAGE gel for analysis.

Immunoblotting. First, 7.5 μl of crude LPS extracts was run on 1.0 mm Tricine SDS polyacrylamide gel electrophoresis (TSDS-PAGE) gel for analysis by immunoblotting. The TSDS-PAGE-separated LPS samples and SDS-PAGE-separated protein samples were transferred onto Immobilon-P polyvinylidene difluoride (PVDF) membrane (Merck-Millipore). For His-tagged protein detection, the primary antibody was Tetra·His antibody (1:1,000) (Qiagen; in 3% [wt/vol] bovine serum albumin [BSA] Tris-buffered saline [TBS]), and the secondary antibody was goat anti-mouse IgG-HRP (1:10,000) (Sigma-Aldrich; in 5% [wt/vol] milk TBS). The blot was developed using Luminata Classico Western HRP substrate (Merck-Millipore). For LPS detection, O:5 serotyping antibody (1:10,000) (Statens Serum Institute; 40272) and *Salmonella* core antigen (1:200) (Insight Biotechnology; 5D12A) were used as the primary antibodies and goat anti-rabbit IgG StarBright Blue700 (1:5,000) (Bio-Rad) and goat anti-mouse IgG (H+L) DyLight 800 (1:5,000) as the respective secondary antibodies. LPS antibodies were diluted in 5% milk phosphate-buffered saline with Tween 20 (PBS-T). The ChemiDoc MP imaging system (Bio-Rad) and Image Lab (Bio-Rad) were used for image capture and analysis. The *in situ* activity of OafA mutant relative to the wild-type protein was derived from quantification of the O:5 signal in each lane, standardized to the intensity of the single O-antigen repeat band for the *Salmonella* core signal on LPS immunoblots. Assay validation demonstrated that <1% of the O:5 signal with respect to the wild type was within the background variation. Variation increased significantly for signal intensities in the higher range; therefore, the O:5 signal recorded between 50 and 100% relative to wild type was not interpreted further.

Expression and purification of OafA-STM$^{C\text{-}term}$ and OafB-SPA$^{C\text{-}term}$. The pETFPP_2 vectors containing the inserted OafA-STM$^{C\text{-}term}$ and OafB-SPA$^{C\text{-}term}$ constructs (Fig. 1) were transformed into Origami (Novagen) *E. coli* for protein expression. Protein expression was carried out as described by Gruszka et al. (85) without the addition of protease inhibitor. The proteins were purified using immobilized metal affinity chromatography with a HisTrap FF column (GE Healthcare) utilizing a His-tag, followed by size exclusion chromatography after His-tag removal, as described by Wojdyla et al. (86); purified protein was eluted in 20 mM Tris-HCl (pH 7.5) and 100 mM NaCl.

Melting temperature of OafA and OafB SGNH domains. The melting temperature of SGNH domains was determined using NanoDSF with a protein concentration of 1 mg/ml in 20 mM TrisHCl (pH 7.5) and 100 mM NaCl. Proteins were heated from 20°C to 95°C with a heating rate of 2°C/min. The fluorescence at 330 and 350 nm was measured every 0.05°C.

***In vitro* acetylesterase activity assay.** The catalytic activity of OafA and OafB C-terminal constructs was confirmed by acetyl esterase activity using pNP-Ac as a substrate. One hundred μl of enzyme solution (10 μM OafA-STM$^{C\text{-}term}$, 40 μM OafB-STM$^{C\text{-}term}$, or 0.04 U/ml acetyl xylan esterase) or appropriate control buffers were added to relevant wells of a 96-well plate and incubated at 37°C for 10 min prior to addition of pNP-Ac. Then, 100 μl of 1 mM pNPA in the corresponding buffer was then added to matching sample and control wells and immediately placed into a plate reader incubated at 37°C. Absorbance at 405 nm was measured at $T = 0$, and then at 5 min intervals.

***In vitro* abequose acetyltransferase activity assay.** Crude LPS extracted from OafA-negative *S.* Typhimurium strain LT2 (Path993) was heated at 100°C for 20 min to inactivate the proteinase K (see above). Heat-treated LPS was mixed 1:1 with KPi buffer (200 mM NaCl, 50 mM potassium phosphate buffer [pH 7.8]). Next, 10 μM OafA-STM$^{C\text{-}term}$ and 20 μM OafB-SPA$^{C\text{-}term}$ were incubated at 4°C in the LPS-KPi mixture with 4 mM pNP-Ac dissolved in ethanol (4% [vol/vol] final concentration in reaction). Samples of the reaction mix were taken after specified time points and inactivated by boiling for 10 min.

Then, 5 μl of LPS reaction samples were loaded onto methanol-activated PVDF membrane using a Bio-Rad Bio-Dot microfiltration apparatus. The protocol for LPS detection with O:5 serotyping antibodies and *Salmonella* core antigen was followed as per immunoblotting, following removal of the membrane from the apparatus after sample loading.

Protein structure analysis. To crystallize OafB-SPA$^{C\text{-}long}$, a hanging-drop vapor diffusion method was used with 20 mg/ml OafB-SPA$^{C\text{-}long}$ in a drop ratio of 1:1 protein:reservoir solution. After incubation for 24 h at 20°C, crystals grown in 100 mM BisTris (pH 5.5), 0.25 M lithium sulfate, and 25% PEG 3350 were cryoprotected by addition of glycerol to a final concentration of 20% and vitrified in liquid nitrogen.

X-ray diffraction data for crystals of OafB-SPA$^{C\text{-}long}$ were collected on beamline I04-1 (Diamond Light Source, UK) at a wavelength of 0.9282 Å using a Pilatus 6M-F detector. Data were integrated with XDS (87) and scaled and merged with AIMLESS (88) via the Xia2 pipeline (89). Fragon molecular replacement (59) used Phaser (90) to place an ideal poly alanine helix of 14 amino acids in length followed by density modification with ACORN (91). ARP-wARP (92) was used for automated chain tracing, and the model was refined using REFMAC 5 (93–98). Manual manipulation of the model between refinement cycles was performed using Coot (99, 100). The final model was evaluated using MolProbity (101) and PDB validate; the secondary structure shown in Fig. 5A was annotated using STRIDE (102).

A homology model of OafA-STM$^{C\text{-}long}$ was produced using SwissModel with the structure of OafB-SPA$^{C\text{-}long}$ as a template (103–107).

Data availability. The atomic coordinates and structure factors have been deposited in the Protein Data Bank (PDB ID code 6SE1).

SUPPLEMENTAL MATERIAL

Supplemental material is available online only.

FIG S1, PDF file, 1.8 MB.
FIG S2, PDF file, 0.7 MB.
FIG S3, PDF file, 0.1 MB.
FIG S4, PDF file, 0.4 MB.
FIG S5, PDF file, 0.5 MB.
FIG S6, PDF file, 0.5 MB.
FIG S7, PDF file, 0.1 MB.
TABLE S1, PDF file, 0.4 MB.
TABLE S2, PDF file, 0.6 MB.
TABLE S3, PDF file, 0.4 MB.

ACKNOWLEDGMENTS

C.R.P. and S.N.T. were supported by a Ph.D. studentship from the Biotechnology and Biological Sciences Research Council White Rose Doctoral Training Program (BB/M011151/1), "Mechanistic Biology and its Strategic Application."

We thank the University of York Technology Facility, Steinar Mannsverk for technical assistance and Jean Whittingham for crystallography support. We thank Diamond Light Source for access to beamline I04-1 (under proposal DLS-MX-13587).

REFERENCES

1. Majowicz SE, Musto J, Scallan E, Angulo FJ, Kirk M, O'Brien SJ, Jones TF, Fazil A, Hoekstra RM, International Collaboration on Enteric Disease 'Burden of Illness' Studies. 2010. The global burden of nontyphoidal Salmonella gastroenteritis. Clin Infect Dis 50:882–889. https://doi.org/10.1086/650733.
2. Hiyoshi H, Tiffany CR, Bronner DN, Bäumler AJ. 2018. Typhoidal Salmonella serovars: ecological opportunity and the evolution of a new pathovar. FEMS Microbiol Rev 42:527–541. https://doi.org/10.1093/femsre/fuy024.
3. Reddy EA, Shaw AV, Crump JA. 2010. Community-acquired bloodstream infections in Africa: a systematic review and meta-analysis. Lancet Infect Dis 10:417–432. https://doi.org/10.1016/S1473-3099(10)70072-4.
4. Crump JA, Luby SP, Mintz ED. 2004. The global burden of typhoid fever. Bull World Health Organ 82:346–353.
5. Lynch MF, Blanton EM, Bulens S, Polyak C, Vojdani J, Stevenson J, Medalla F, Barzilay E, Joyce K, Barrett T, Mintz ED. 2009. Typhoid fever in the United States, 1999–2006. JAMA 302:859. https://doi.org/10.1001/jama.2009.1229.
6. Boore AL, Hoekstra RM, Iwamoto M, Fields PI, Bishop RD, Swerdlow DL. 2015. Salmonella enterica infections in the United States and assessment of coefficients of variation: a novel approach to identify epidemiologic characteristics of individual serotypes, 1996–2011. PLoS One 10:e0145416. https://doi.org/10.1371/journal.pone.0145416.
7. Liu B, Knirel YA, Feng L, Perepelov AV, Senchenkova SN, Reeves PR, Wang L. 2014. Structural diversity in Salmonella O antigens and its genetic basis. FEMS Microbiol Rev 38:56–89. https://doi.org/10.1111/1574-6976.12034.
8. Raetz C, Whitfield C. 2002. Lipopolysaccharide endotoxins. Annu Rev Biochem 71:635–700. https://doi.org/10.1146/annurev.biochem.71.110601.135414.
9. Kintz E, Davies MR, Hammarlöf DL, Canals R, Hinton JCD, van der Woude MW. 2015. A BTP1 prophage gene present in invasive non-typhoidal Salmonella determines composition and length of the O-antigen of the lipopolysaccharide. Mol Microbiol 96:263–275. https://doi.org/10.1111/mmi.12933.
10. Kintz E, Heiss C, Black I, Donohue N, Brown N, Davies MR, Azadi P, Baker S, Kaye PM, van der Woude M. 2017. Salmonella Typhi lipopolysaccharide O-antigen modifications impact on serum resistance and antibody recognition. Infect Immun 85:e01021-16. https://doi.org/10.1128/IAI.01021-16.
11. Kim ML, Slauch JM. 1999. Effect of acetylation (O-factor 5) on the polyclonal antibody response to Salmonella typhimurium O-antigen. FEMS Immunol Med Microbiol 26:83–92. https://doi.org/10.1111/j.1574-695X.1999.tb01375.x.
12. Fierer J, Guiney DG. 2001. Diverse virulence traits underlying different clinical outcomes of Salmonella infection. J Clin Invest 107:775–780. https://doi.org/10.1172/JCI12561.
13. Moynihan PJ, Clarke AJ. 2011. O-acetylated peptidoglycan: controlling the activity of bacterial autolysins and lytic enzymes of innate immune systems. Int J Biochem Cell Biol 43:1655–1659. https://doi.org/10.1016/j.biocel.2011.08.007.
14. Bera A, Herbert S, Jakob A, Vollmer W, Götz F. 2005. Why are pathogenic staphylococci so lysozyme resistant? The peptidoglycan O-acetyltransferase OatA is the major determinant for lysozyme resistance of Staphylococcus aureus. Mol Microbiol 55:778–787. https://doi.org/10.1111/j.1365-2958.2004.04446.x.
15. Davis EO, Evans IJ, Johnston AWB. 1988. Identification of nodX, a gene that allows Rhizobium leguminosarum biovar viciae strain TOM to

nodulate Afghanistan peas. Mol Gen Genet 212:531–535. https://doi.org/10.1007/BF00330860.
16. Verma NK, Brandt JM, Verma DJ, Lindberg AA. 1991. Molecular characterization of the O-acetyl transferase gene of converting bacteriophage SF6 that adds group antigen 6 to Shigella flexneri. Mol Microbiol 5:71–75. https://doi.org/10.1111/j.1365-2958.1991.tb01827.x.
17. Slauch JM, Lee AA, Mahan MJ, Mekalanos JJ. 1996. Molecular characterization of the oafA locus responsible for acetylation of Salmonella typhimurium O-antigen: OafA is a member of a family of integral membrane trans-acylases. J Bacteriol 178:5904–5909. https://doi.org/10.1128/jb.178.20.5904-5909.1996.
18. Clark CA, Beltrame J, Manning PA. 1991. The oac gene encoding a lipopolysaccharide O-antigen acetylase maps adjacent to the integrase-encoding gene on the genome of Shigella flexneri bacteriophage Sf6. Gene 107:43–52. https://doi.org/10.1016/0378-1119(91)90295-m.
19. Dalrymple BP, Cybinski DH, Layton I, McSweeney CS, Xue GP, Swadling YJ, Lowry JB. 1997. Three Neocallimastix patriciarum esterases associated with the degradation of complex polysaccharides are members of a new family of hydrolases. Microbiology 143:2605–2614. https://doi.org/10.1099/00221287-143-8-2605.
20. Mølgaard A, Kauppinen S, Larsen S. 2000. Rhamnogalacturonan acetylesterase elucidates the structure and function of a new family of hydrolases. Structure 8:373–383. https://doi.org/10.1016/s0969-2126(00)00118-0.
21. Lombard V, Golaconda Ramulu H, Drula E, Coutinho PM, Henrissat B. 2014. The carbohydrate-active enzymes database (CAZy) in 2013. Nucleic Acids Res 42:D490–495. https://doi.org/10.1093/nar/gkt1178.
22. Akoh CC, Lee G-C, Liaw Y-C, Huang T-H, Shaw J-F. 2004. GDSL family of serine esterases/lipases. Prog Lipid Res 43:534–552. https://doi.org/10.1016/j.plipres.2004.09.002.
23. Davies MR, Broadbent SE, Harris SR, Thomson NR, van der Woude MW. 2013. Horizontally acquired glycosyltransferase operons drive salmonellae lipopolysaccharide diversity. PLoS Genet 9:e1003568. https://doi.org/10.1371/journal.pgen.1003568.
24. Slauch JM, Mahan MJ, Michetti P, Neutra MR, Mekalanos JJ. 1995. Acetylation (O-factor 5) affects the structural and immunological properties of Salmonella typhimurium lipopolysaccharide O antigen. Infect Immun 63:437–441. https://doi.org/10.1128/IAI.63.2.437-441.1995.
25. Grimont P, Weill F-X (ed). 2008. Antigenic formulae of the Salmonella serovars. WHO Collaborating Centre for Reference and Research on Salmonella, Paris, France.
26. Issenhuth-Jeanjean S, Roggentin P, Mikoleit M, Guibourdenche M, de Pinna E, Nair S, Fields PI, Weill FX. 2014. Supplement 2008–2010 (no. 48) to the White-Kauffmann-Le Minor scheme. Res Microbiol 165:526–530. https://doi.org/10.1016/j.resmic.2014.07.004.
27. Lanzilao L, Stefanetti G, Saul A, MacLennan CA, Micoli F, Rondini S. 2015. Strain selection for generation of O-antigen-based glycoconjugate vaccines against invasive nontyphoidal Salmonella disease. PLoS One 10:e0139847. https://doi.org/10.1371/journal.pone.0139847.
28. Mitchell A, Chang H-Y, Daugherty L, Fraser M, Hunter S, Lopez R, McAnulla C, McMenamin C, Nuka G, Pesseat S, Sangrador-Vegas A, Scheremetjew M, Rato C, Yong S-Y, Bateman A, Punta M, Attwood TK, Sigrist CJA, Redaschi N, Rivoire C, Xenarios I, Kahn D, Guyot D, Bork P, Letunic I, Gough J, Oates M, Haft D, Huang H, Natale DA, Wu CH, Orengo C, Sillitoe I, Mi H, Thomas PD, Finn RD. 2015. The InterPro protein families database: the classification resource after 15 years. Nucleic Acids Res 43:D213–21. https://doi.org/10.1093/nar/gku1243.
29. Finn RD, Bateman A, Clements J, Coggill P, Eberhardt RY, Eddy SR, Heger A, Hetherington K, Holm L, Mistry J, Sonnhammer ELL, Tate J, Punta M. 2014. Pfam: the protein families database. Nucleic Acids Res 42:D222–30. https://doi.org/10.1093/nar/gkt1223.
30. Krogh A, Larsson B, Von Heijne G, Sonnhammer EL. 2001. Predicting transmembrane protein topology with a hidden Markov model: application to complete genomes. J Mol Biol 305:567–580. https://doi.org/10.1006/jmbi.2000.4315.
31. Thanweer F, Verma NK. 2012. Identification of critical residues of the serotype modifying O-acetyltransferase of Shigella flexneri. BMC Biochem 13:13. https://doi.org/10.1186/1471-2091-13-13.
32. Crisóstomo MI, Vollmer W, Kharat AS, Inhülsen S, Gehre F, Buckenmaier S, Tomasz A. 2006. Attenuation of penicillin resistance in a peptidoglycan O-acetyl transferase mutant of Streptococcus pneumoniae. Mol Microbiol 61:1497–1509. https://doi.org/10.1111/j.1365-2958.2006.05340.x.
33. Laaberki MH, Pfeffer J, Clarke AJ, Dworkin J. 2011. O-acetylation of peptidoglycan is required for proper cell separation and S-layer anchoring in Bacillus anthracis. J Biol Chem 286:5278–5288. https://doi.org/10.1074/jbc.M110.183236.
34. Buendia AM, Enenkel B, Köplin R, Niehaus K, Arnold W, Pühler A. 1991. The Rhizobium meliloti exoZl exoB fragment of megaplasmid 2: ExoB functions as a UDP-glucose 4-epimerase and ExoZ shows homology to NodX of Rhizobium leguminosarum biovar viciae strain TOM. Mol Microbiol 5:1519–1530. https://doi.org/10.1111/j.1365-2958.1991.tb00799.x.
35. Katzen F, Ferreiro DU, Oddo CG, Ielmini MV, Becker A, Pühler A, Ielpi L. 1998. Xanthomonas campestris pv. campestris gum mutants: effects on xanthan biosynthesis and plant virulence. J Bacteriol 180:1607–1617. https://doi.org/10.1128/JB.180.7.1607-1617.1998.
36. Fox KL, Yildirim HH, Deadman ME, Schweda EKH, Moxon ER, Hood DW. 2005. Novel lipopolysaccharide biosynthetic genes containing tetranucleotide repeats in Haemophilus influenzae, identification of a gene for adding O-acetyl groups. Mol Microbiol 58:207–216. https://doi.org/10.1111/j.1365-2958.2005.04814.x.
37. Zou CH, Knirel YA, Helbig JH, Zähringer U, Mintz CS. 1999. Molecular cloning and characterization of a locus responsible for O acetylation of the O polysaccharide of Legionella pneumophila serogroup 1 lipopolysaccharide. J Bacteriol 181:4137–4141. https://doi.org/10.1128/JB.181.13.4137-4141.1999.
38. Aubry C, Goulard C, Nahori MA, Cayet N, Decalf J, Sachse M, Boneca IG, Cossart P, Dussurget O. 2011. OatA, a peptidoglycan O-acetyltransferase involved in Listeria monocytogenes immune escape, is critical for virulence. J Infect Dis 204:731–740. https://doi.org/10.1093/infdis/jir396.
39. Kahler CM, Lyons-Schindler S, Choudhury B, Glushka J, Carlson RW, Stephens DS. 2006. O-acetylation of the terminal N-acetylglucosamine of the lipooligosaccharide inner core in Neisseria meningitidis: influence on inner core structure and assembly. J Biol Chem 281:19939–19948. https://doi.org/10.1074/jbc.M601308200.
40. Bernard E, Rolain T, Courtin P, Guillot A, Langella P, Hols P, Chapot-Chartier M-P. 2011. Characterization of O-acetylation of N-acetylglucosamine: a novel structural variation of bacterial peptidoglycan. J Biol Chem 286:23950–23958. https://doi.org/10.1074/jbc.M111.241414.
41. Pacios Bras C, Jordá MA, Wijfjes A H, Harteveld M, Stuurman N, Thomas-Oates JE, Spaink HP. 2000. A Lotus japonicus nodulation system based on heterologous expression of the fucosyl transferase NodZ and the acetyl transferase NoIL in Rhizobium leguminosarum. Mol Plant Microbe Interact 13:475–479. https://doi.org/10.1094/MPMI.2000.13.4.475.
42. Brett PJ, Burtnick MN, Heiss C, Azadi P, DeShazer D, Woods DE, Gherardini FC. 2011. Burkholderia thailandensis oacA mutants facilitate the expression of Burkholderia mallei-like O polysaccharides. Infect Immun 79:961–969. https://doi.org/10.1128/IAI.01023-10.
43. Wang J, Knirel YA, Lan R, Senchenkova SN, Luo X, Perepelov AV, Wang Y, Shashkov AS, Xu J, Sun Q. 2014. Identification of an O-acyltransferase gene (oacB) that mediates 3- and 4-O-acetylation of rhamnose III in Shigella flexneri O antigens. J Bacteriol 196:1525–1531. https://doi.org/10.1128/JB.01393-13.
44. Knirel YA, Wang J, Luo X, Senchenkova SN, Lan R, Shpirt AM, Du P, Shashkov AS, Zhang N, Xu J, Sun Q. 2014. Genetic and structural identification of an O-acyltransferase gene (oacC) responsible for the 3/4-O-acetylation on rhamnose III in Shigella flexneri serotype 6. BMC Microbiol 14:266. https://doi.org/10.1186/s12866-014-0266-7.
45. Sun Q, Knirel YA, Wang J, Luo X, Senchenkova SN, Lan R, Shashkov AS, Xu J. 2014. Serotype-converting bacteriophage SfII encodes an acyltransferase protein that mediates 6-O-acetylation of GlcNAc in Shigella flexneri O-antigens, conferring on the host a novel O-antigen epitope. J Bacteriol 196:3656–3666. https://doi.org/10.1128/JB.02009-14.
46. Cogez V, Gak E, Puskas A, Kaplan S, Bohin JP. 2002. The opgGIH and opgC genes of Rhodobacter sphaeroides form an operon that controls backbone synthesis and succinylation of osmoregulated periplasmic glucans. Eur J Biochem 269:2473–2484. https://doi.org/10.1046/j.1432-1033.2002.02907.x.
47. Bontemps-Gallo S, Madec E, Robbe-Masselot C, Souche E, Dondeyne J, Lacroix J-M. 2016. The opgC gene is required for OPGs succinylation and is osmoregulated through RcsCDB and EnvZ/OmpR in the phytopathogen Dickeya dadantii. Sci Rep 6:19619. https://doi.org/10.1038/srep19619.
48. Hong Y, Duda KA, Cunneen MM, Holst O, Reeves PR. 2013. The WbaK acetyltransferase of Salmonella enterica group E gives insights into O antigen evolution. Microbiology 159:2316–2322. https://doi.org/10.1099/mic.0.069823-0.

49. Brett PJ, Burtnick M, Woods D. 2003. The wbiA locus is required for the 2-O-acetylation of lipopolysaccharides expressed by Burkholderia pseudomallei and Burkholderia thailandensis. FEMS Microbiol Lett 218:323–328. https://doi.org/10.1111/j.1574-6968.2003.tb11536.x.
50. Geno KA, Saad JS, Nahm MH. 2017. Discovery of novel pneumococcal serotype 35D, a natural WciG-deficient variant of serotype 35B. J Clin Microbiol 55:1416–1425. https://doi.org/10.1128/JCM.00054-17.
51. Calix JJ, Nahm MH. 2010. A new pneumococcal serotype, 11E, has a variably inactivated wcjE gene. J Infect Dis 202:29–38. https://doi.org/10.1086/653123.
52. Kajimura J, Rahman A, Hsu J, Evans MR, Gardner KH, Rick PD. 2006. O acetylation of the enterobacterial common antigen polysaccharide is catalyzed by the product of the yiaH gene of Escherichia coli K-12. J Bacteriol 188:7542–7550. https://doi.org/10.1128/JB.00783-06.
53. Veiga P, Bulbarela-Sampieri C, Furlan S, Maisons A, Chapot-Chartier M-P, Erkelenz M, Mervelet P, Noirot P, Frees D, Kuipers OP, Kok J, Gruss A, Buist G, Kulakauskas S. 2007. SpxB regulates O-acetylation-dependent resistance of Lactococcus lactis peptidoglycan to hydrolysis. J Biol Chem 282:19342–19354. https://doi.org/10.1074/jbc.M611308200.
54. Menéndez N, Nur-e-Alam M, Braña AF, Rohr J, Salas JA, Méndez C. 2004. Biosynthesis of the antitumor chromomycin A3 in Streptomyces griseus: analysis of the gene cluster and rational design of novel chromomycin analogs. Chem Biol 11:21–32. https://doi.org/10.1016/j.chembiol.2003.12.011.
55. Warren MJ, Roddam LF, Power PM, Terry TD, Jennings MP. 2004. Analysis of the role of pgll in pilin glycosylation of Neisseria meningitidis. FEMS Immunol Med Microbiol 41:43–50. https://doi.org/10.1016/j.femsim.2004.01.002.
56. Hauser E, Junker E, Helmuth R, Malorny B. 2011. Different mutations in the oafA gene lead to loss of O5-antigen expression in Salmonella enterica serovar Typhimurium. J Appl Microbiol 110:248–253. https://doi.org/10.1111/j.1365-2672.2010.04877.x.
57. Thanweer F, Tahiliani V, Korres H, Verma NK. 2008. Topology and identification of critical residues of the O-acetyltransferase of serotype-converting bacteriophage, SF6, of Shigella flexneri. Biochem Biophys Res Commun 375:581–585. https://doi.org/10.1016/j.bbrc.2008.08.069.
58. Ravenscroft N, Cescutti P, Gavini M, Stefanetti G, Maclennan CA, Martin LB, Micoli F. 2015. Structural analysis of the O-acetylated O-polysaccharide isolated from Salmonella Paratyphi A and used for vaccine preparation. Carbohydr Res 404:108–116. https://doi.org/10.1016/j.carres.2014.12.002.
59. Jenkins HT. 2018. Fragon: rapid high-resolution structure determination from ideal protein fragments. Acta Crystallogr D Struct Biol 74:205–214. https://doi.org/10.1107/S2059798318002292.
60. Sychantha D, Jones CS, Little DJ, Moynihan PJ, Robinson H, Galley NF, Roper DI, Dowson CG, Howell PL, Clarke AJ. 2017. In vitro characterization of the antivirulence target of Gram-positive pathogens, peptidoglycan O-acetyltransferase A (OatA). PLoS Pathog 13:e1006667. https://doi.org/10.1371/journal.ppat.1006667.
61. Lee L-C, Lee Y-L, Leu R-J, Shaw J-F. 2006. Functional role of catalytic triad and oxyanion hole-forming residues on enzyme activity of Escherichia coli thioesterase I/protease I/phospholipase L1. Biochem J 397:69–76. https://doi.org/10.1042/BJ20051645.
62. Moynihan PJ, Clarke AJ. 2014. Substrate specificity and kinetic characterization of peptidoglycan O-acetyltransferase B from Neisseria gonorrhoeae. J Biol Chem 289:16748–16760. https://doi.org/10.1074/jbc.M114.567388.
63. Pfeffer JM, Weadge JT, Clarke AJ. 2013. Mechanism of action of Neisseria gonorrhoeae O-acetylpeptidoglycan esterase, an SGNH serine esterase. J Biol Chem 288:2605–2613. https://doi.org/10.1074/jbc.M112.436352.
64. Baker P, Ricer T, Moynihan PJ, Kitova EN, Walvoort MTC, Little DJ, Whitney JC, Dawson K, Weadge JT, Robinson H, Ohman DE, Codée JDC, Klassen JS, Clarke AJ, Howell PL. 2014. P. aeruginosa SGNH hydrolase-like proteins AlgJ and AlgX have similar topology but separate and distinct roles in alginate acetylation. PLoS Pathog 10:e1004334. https://doi.org/10.1371/journal.ppat.1004334.
65. Moynihan PJ, Clarke AJ. 2013. Assay for peptidoglycan O-acetyltransferase: a potential new antibacterial target. Anal Biochem 439:73–79. https://doi.org/10.1016/j.ab.2013.04.022.
66. Menéndez N, Nur-e-Alam M, Braña AF, Rohr J, Salas JA, Méndez C. 2004. Tailoring modification of deoxysugars during biosynthesis of the antitumour drug chromomycin A3 by Streptomyces griseus ssp. griseus. Mol Microbiol 53:903–915. https://doi.org/10.1111/j.1365-2958.2004.04166.x.
67. Arisawa A, Kawamura N, Tsunekawa H, Okamura K, Tone H, Okamoto R. 1993. Cloning and nucleotide sequences of two genes involved in the 4″-O-acylation of macrolide antibiotics from Streptomyces thermotolerans. Biosci Biotechnol Biochem 57:2020–2025. https://doi.org/10.1271/bbb.57.2020.
68. Takamura Y, Nomura G. 1988. Changes in the intracellular concentration of acetyl-CoA and malonyl-CoA in relation to the carbon and energy metabolism of Escherichia coli K12. J Gen Microbiol 134:224:2249–2253. https://doi.org/10.1099/00221287-134-8-2249.
69. Krivoruchko A, Zhang Y, Siewers V, Chen Y, Nielsen J. 2015. Microbial acetyl-CoA metabolism and metabolic engineering. Metab Eng 28:28–42. https://doi.org/10.1016/j.ymben.2014.11.009.
70. Wu D, Hersh LB. 1995. Identification of an active site arginine in rat choline acetyltransferase by alanine scanning mutagenesis. J Biol Chem 270:29111–29116. https://doi.org/10.1074/jbc.270.49.29111.
71. Jogl G, Hsiao Y-S, Tong L. 2004. Structure and function of carnitine acyltransferases. Ann N Y Acad Sci 1033:17–29. https://doi.org/10.1196/annals.1320.002.
72. Calix JJ, Oliver MB, Sherwood LK, Beall BW, Hollingshead SK, Nahm MH. 2011. Streptococcus pneumoniae serotype 9A isolates contain diverse mutations to wcjE that result in variable expression of serotype 9V-specific epitope. J Infect Dis 204:1585–1595. https://doi.org/10.1093/infdis/jir593.
73. Ma D, Wang Z, Merrikh CN, Lang KS, Lu P, Li X, Merrikh H, Rao Z, Xu W. 2018. Crystal structure of a membrane-bound O-acyltransferase. Nature 562:286–290. https://doi.org/10.1038/s41586-018-0568-2.
74. Roset MS, Ciocchini AE, Ugalde RA, Inon de Iannino N. 2006. The Brucella abortus cyclic β-1,2-glucan virulence factor is substituted with O-ester-linked succinyl residues. J Bacteriol 188:5003–5013. https://doi.org/10.1128/JB.00086-06.
75. Cong L, Piepersberg W. 2007. Cloning and characterization of genes encoded in dTDP-D-mycaminose biosynthetic pathway from a midecamycin-producing strain, streptomyces mycarofaciens. Acta Biochim Biophys Sin (Shanghai) 39:187–193. https://doi.org/10.1111/j.1745-7270.2007.00265.x.
76. Moynihan PJ, Clarke AJ. 2010. O-acetylation of peptidoglycan in Gram-negative bacteria: identification and characterization of peptidoglycan O-acetyltransferase in Neisseria gonorrhoeae. J Biol Chem 285:13264–13273. https://doi.org/10.1074/jbc.M110.107086.
77. Bernard E, Rolain T, David B, André G, Dupres V, Dufrêne YF, Hallet B, Chapot-Chartier M-P, Hols P. 2012. Dual role for the O-acetyltransferase OatA in peptidoglycan modification and control of cell septation in Lactobacillus plantarum. PLoS One 7:e47893. https://doi.org/10.1371/journal.pone.0047893.
78. Baranwal G, Mohammad M, Jarneborn A, Reddy BR, Golla A, Chakravarty S, Biswas L, Götz F, Shankarappa S, Jin T, Biswas R. 2017. Impact of cell wall peptidoglycan O-acetylation on the pathogenesis of Staphylococcus aureus in septic arthritis. Int J Med Microbiol 307:388–397. https://doi.org/10.1016/j.ijmm.2017.08.002.
79. Knirel YA, Prokhorov NS, Shashkov AS, Ovchinnikova OG, Zdorovenko EL, Liu B, Kostryukova ES, Larin AK, Golomidova AK, Letarov AV. 2015. Variations in O-antigen biosynthesis and O-acetylation associated with altered phage sensitivity in Escherichia coli 4s. J Bacteriol 197:905–912. https://doi.org/10.1128/JB.02398-14.
80. Lizak C, Gerber S, Numao S, Aebi M, Locher KP. 2011. X-ray structure of a bacterial oligosaccharyltransferase. Nature 474:350–355. https://doi.org/10.1038/nature10151.
81. Vora M, Shah M, Ostafi S, Onken B, Xue J, Ni JZ, Gu S, Driscoll M. 2013. Deletion of microRNA-80 activates dietary restriction to extend C. elegans healthspan and lifespan. PLoS Genet 9:e1003737. https://doi.org/10.1371/journal.pgen.1003737.
82. Dzitoyeva S, Dimitrijevic N, Manev H. 2003. Identification of a novel Drosophila gene, beltless, using injectable embryonic and adult RNA interference (RNAi). BMC Genomics 4:33. https://doi.org/10.1186/1471-2164-4-33.
83. Notredame C, Higgins DG, Heringa J. 2000. T-coffee: a novel method for fast and accurate multiple sequence alignment. J Mol Biol 302:205–217. https://doi.org/10.1006/jmbi.2000.4042.
84. Källberg M, Margaryan G, Wang S, Ma J, Xu J. 2014. RaptorX server: a resource for template-based protein structure modeling. Methods Mol Biol 1137:17–27. https://doi.org/10.1007/978-1-4939-0366-5_2.
85. Gruszka DT, Whelan F, Farrance OE, Fung HKH, Paci E, Jeffries CM, Svergun DI, Baldock C, Baumann CG, Brockwell DJ, Potts JR, Clarke J. 2015. Cooperative folding of intrinsically disordered domains drives

assembly of a strong elongated protein. Nat Commun 6:7271. https://doi.org/10.1038/ncomms8271.
86. Gruszka DT, Wojdyla JA, Bingham RJ, Turkenburg JP, Manfield IW, Steward A, Leech AP, Geoghegan JA, Foster TJ, Clarke J, Potts JR. 2012. Staphylococcal biofilm-forming protein has a contiguous rod-like structure. Proc Natl Acad Sci U S A 109:E1011–E1018. https://doi.org/10.1073/pnas.1119456109.
87. Kabsch W. 2010. *XDS*. Acta Crystallogr D Biol Crystallogr 66:125–132. https://doi.org/10.1107/S0907444909047337.
88. Evans PR, Murshudov GN. 2013. How good are my data and what is the resolution? Acta Crystallogr D Biol Crystallogr 69:1204–1214. https://doi.org/10.1107/S0907444913000061.
89. Winter G. 2010. xia2: an expert system for macromolecular crystallography data reduction. J Appl Crystallogr 43:186–190. https://doi.org/10.1107/S0021889809045701.
90. McCoy AJ, Grosse-Kunstleve RW, Adams PD, Winn MD, Storoni LC, Read RJ. 2007. Phaser crystallographic software. J Appl Crystallogr 40:658–674. https://doi.org/10.1107/S0021889807021206.
91. Jia-Xing Y, Woolfson MM, Wilson KS, Dodson EJ. 2005. A modified ACORN to solve protein structures at resolutions of 1.7 A or better. Acta Crystallogr D Biol Crystallogr 61:1465–1475. https://doi.org/10.1107/S090744490502576X.
92. Perrakis A, Morris R, Lamzin VS. 1999. Automated protein model building combined with iterative structure refinement. Nat Struct Biol 6:458–463. https://doi.org/10.1038/8263.
93. Murshudov GN, Skubák P, Lebedev AA, Pannu NS, Steiner RA, Nicholls RA, Winn MD, Long F, Vagin AA, IUCr. 2011. REFMAC 5 for the refinement of macromolecular crystal structures. Acta Crystallogr D Biol Crystallogr 67:355–367. https://doi.org/10.1107/S0907444911001314.
94. Vagin AA, Steiner RA, Lebedev AA, Potterton L, McNicholas S, Long F, Murshudov GN. 2004. REFMAC 5 dictionary: organization of prior chemical knowledge and guidelines for its use. Acta Crystallogr D Biol Crystallogr 60:2184–2195. https://doi.org/10.1107/S0907444904023510.
95. Nicholls RA, Long F, Murshudov GN. 2012. Low-resolution refinement tools in REFMAC 5. Acta Crystallogr D Biol Crystallogr 68:404–417. https://doi.org/10.1107/S090744491105606X.
96. Murshudov GN, Vagin AA, Lebedev A, Wilson KS, Dodson EJ. 1999. Efficient anisotropic refinement of macromolecular structures using FFT. Acta Crystallogr D Biol Crystallogr 55:247–255. https://doi.org/10.1107/S0907444499801405X.
97. Winn MD, Murshudov GN, Papiz MZ. 2003 Macromolecular TLS Refinement in REFMAC at Moderate Resolutions, Methods Enzymol 374:300–321. https://doi.org/10.1016/S0076-6879(03)74014-2.
98. Murshudov GN, Vagin AA, Dodson EJ. 1997. Refinement of macromolecular structures by the maximum-likelihood method. Acta Crystallogr D Biol Crystallogr 53:240–255. https://doi.org/10.1107/S0907444996012255.
99. Emsley P, Cowtan K. 2004. *Coot*: model-building tools for molecular graphics. Acta Crystallogr D Biol Crystallogr 60:2126–2132. https://doi.org/10.1107/S0907444904019158.
100. Emsley P, Lohkamp B, Scott WG, Cowtan K. 2010. Features and development of Coot. Acta Crystallogr D Biol Crystallogr 66:486–501. https://doi.org/10.1107/S0907444910007493.
101. Chen VB, Arendall WB, Headd JJ, Keedy DA, Immormino RM, Kapral GJ, Murray LW, Richardson JS, Richardson DC, Richardson DC. 2010. MolProbity: all-atom structure validation for macromolecular crystallography. Acta Crystallogr D Biol Crystallogr 66:12–21. https://doi.org/10.1107/S0907444909042073.
102. Heinig M, Frishman D. 2004. STRIDE: a Web server for secondary structure assignment from known atomic coordinates of proteins. Nucleic Acids Res 32:W500–W502. https://doi.org/10.1093/nar/gkh429.
103. Bertoni M, Kiefer F, Biasini M, Bordoli L, Schwede T. 2017. Modeling protein quaternary structure of homo- and hetero-oligomers beyond binary interactions by homology. Sci Rep 7:10480. https://doi.org/10.1038/s41598-017-09654-8.
104. Waterhouse A, Bertoni M, Bienert S, Studer G, Tauriello G, Gumienny R, Heer FT, de Beer TAP, Rempfer C, Bordoli L, Lepore R, Schwede T. 2018. SWISS-MODEL: homology modelling of protein structures and complexes. Nucleic Acids Res 46:W296–W303. https://doi.org/10.1093/nar/gky427.
105. Bienert S, Waterhouse A, de Beer TAP, Tauriello G, Studer G, Bordoli L, Schwede T. 2017. The SWISS-MODEL Repository: new features and functionality. Nucleic Acids Res 45:D313–D319. https://doi.org/10.1093/nar/gkw1132.
106. Benkert P, Biasini M, Schwede T. 2011. Toward the estimation of the absolute quality of individual protein structure models. Bioinformatics 27:343–350. https://doi.org/10.1093/bioinformatics/btq662.
107. Guex N, Peitsch MC, Schwede T. 2009. Automated comparative protein structure modeling with SWISS-MODEL and Swiss-PdbViewer: a historical perspective. Electrophoresis 30:S162–S173. https://doi.org/10.1002/elps.200900140.